Article:
Kunimatsu, Kazuma, Tsuchiya, Tomoki, Roy, Tufan et al. (5 more authors) (2020) Magnetic tunnel junctions with metastable bcc Co3Mn electrodes. Applied Physics Express. 083007. ISSN 1882-0786

https://doi.org/10.35848/1882-0786/aba883

Magnetic tunnel junctions with metastable bcc Co_3Mn electrodes

Kazuma KUNIMATSU[1,2], Tomoki TSUCHIYA[3,4], Tufan ROY[5], Kelvin ELPHICK[6], Tomohiro ICHINOSE[2], Masahito TSUJIKAWA[5,4], Atsufumi HIROHATA[6], Masafumi SHIRAI[5,4,3], Shigemi MIZUKAMI[2,4,3]*,

[1]*Department of Applied Physics, Tohoku Univ., Aoba 6-6-05, Sendai 980-8579, Japan* [2]*WPI Advanced Institute for Material Research, Tohoku Univ., Katahira 2-1-1, Sendai 980-8577, Japan* [3]*Center for Science and Innovation in Spintronics (CSIS), Core Research Cluster (CRC), Tohoku University, Sendai 980-8577, Japan* [4]*Center for Spintronics Research Network (CSRN), Tohoku University, Sendai 980-8577, Japan* [5]*Research Institute of Electrical Communication (RIEC), Tohoku University, Sendai 980-8579, Japan* [6]*Department of Electronic Engineering, University of York, York YO10 5DD, United Kingdom*

We studied magnetic tunnel junctions (MTJs) with a MgO(001) barrier and metastable bcc Co_3Mn(001) disordered alloy electrodes. A tunnel magnetoresistance (TMR) ratio was approximately 200–250% observed at room temperature. We successfully observed the TMR ratio greater than 600% at 10 K which was higher than the past reported value of MgO-based MTJs with ultrathin bcc Co(001) electrodes. However our experimental value was still much lower than the past theoretical prediction in bcc Co/MgO/Co(001) MTJs. We discuss some differences in the bulk band structure affecting the TMR effect for bcc Co and bcc Co_3Mn.

A magnetic tunnel junction (MTJ) is a key device for spintronics, being utilized in sensors, hard drives, and memories.[1–3] Current standard MTJs are composed of FeCo(B) alloy electrodes and a MgO barrier,[4] which exhibit a large tunnel magnetoresistance (TMR) effect, up to 604% at room temperature (RT) after high-temperature annealing.[5] Recently some groups proposed MTJ-based non-von-Neumann computing circuits, in which one of the requirements for MTJs is a huge TMR effect, typically 500-1000% at RT.[6–8] Most of the previous works focused on bcc FeCo(B)[4,5,9–17] and Co_2-based full Heusler alloys[18–22] for magnetic electrodes to obtain large TMR effects. This is due to the theoretical prediction of the coherent tunneling for MgO-based MTJs with Fe(001) or B2 ordered FeCo(001) electrodes[23,24] and because of the half-metallic electronic structures for Co_2-based full Heusler alloys.[25] In fact, the experimental TMR ratios reached 1.1–2.6×10^3% at low temperature (LT) in MgO-based MTJs with FeCo(B)(001)[5] or some Heusler alloy electrodes such as Co_2MnSi(001),[21] whereas those values were significantly reduced at RT. Hence further research on materials and physics for MTJs is crucial to achieve such huge TMR effect at RT.

The TMR ratio more than 10^4% due to the coherent tunneling has also been predicted in MgO-based MTJs with bcc Co(001) electrodes, which is much higher than those with Fe(001) electrodes.[26] Indeed, Yuasa *et al.* reported that MgO-based MTJs with the ultrathin bcc Co(001) electrodes exhibited the TMR ratio of 410% at RT and 507% at LT.[27] However there were no other experimental reports on the high TMR effect in MgO-based MTJs with bcc Co(001) electrodes and some questions were also raised.[13,14] It is difficult, in general, to obtain nm-thick and single-phase bcc Co films.[12,14,27–31] This would be because bcc Co is not a true metastable phase of bulk Co, as theoretically suggested.[32] Thus the research on MgO-based MTJs with other bcc Co alloy electrodes would shed light on this issue.

One interesting alloy is the metastable bcc $Co_{1-x}Mn_x$.[33–36] This metastable phase was first reported as films which were grown on GaAs(001) with molecular beam epitaxy (MBE),[33] and those bcc film thickness can be extended up to ≃55 nm for approximately $x = 0.25$.[33] The bcc films have also been grown on MgO(001) with MBE, and their X-ray magnetic circular dichroism indicated that the magnetic moment of Mn is ferromagnetically coupled to that of Co and is maximized at approximately $x = 0.25$.[35] The Curie temperatures T_c for the bcc films with $x > 0.33$ have been investigated.[34] We reported 10-nm-thick bcc films with $x = 0.25$ fabricated by sputtering whose saturation magnetization is approximately 1600 emu/cm^3, which is larger than that of bulk Co, about 1400 emu/cm^3.[36] We also preliminarily reported the TMR effect in Co_3Mn/MgO/FeCo(B)(001) pseudo-spin valve-type MTJs, and its ratio was 150% at RT.[36] Note that a fcc or hcp structure is stable in Co-rich $Co_{1-x}Mn_x$ binaries.[37–40] For these phases the magnetizations are remarkably reduced with increasing x due to the antiferromagnetic coupling of magnetic moments for Co and Mn, then fcc $Co_{1-x}Mn_x$ alloys become antiferromagnets at $x = 0.3 - 0.4$. Thus the magnetism of the metastable bcc and stable fcc/hcp phases of $Co_{1-x}Mn_x$ are quite distinct at $x = 0.2 - 0.4$.

In this letter we report successful observation of the high TMR ratio in the Co_3Mn/MgO/Co_3Mn(001) MTJs. The TMR ratios of approximately 200–250% were observed at RT. More importantly, the TMR ratio of greater than 600% at LT was observed, which was higher than the above-mentioned value in MgO-based MTJs with the ultrathin bcc Co(001) electrodes.[27] It should be noted that the crystal structure of the metastable Co_3Mn studied here is $A2$, namely the disordered bcc as mentioned above. This is contrast to the past study on MgO-based MTJs with metastable $B2$ ordered Fe_3Sn.[41,42]

Sample films were deposited on MgO(001) single crystal substrates using a conventional magnetron sputtering with a base pressure of 2×10^{-7} Pa, as similarly employed previously.[36,43–47] We fabricated and

*E-mail: shigemi.mizukami.a7@tohoku.ac.jp

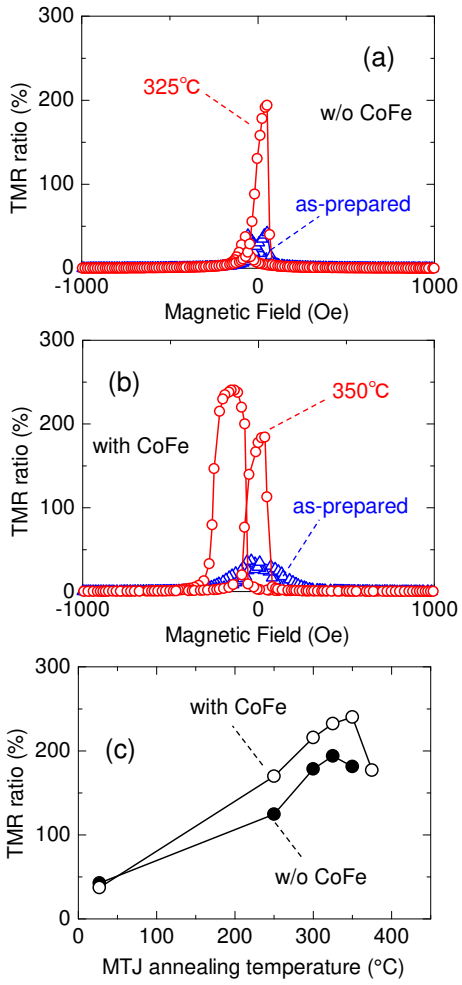

Fig. 1. The typical MR curves measured at RT for $Co_3Mn/MgO/Co_3Mn(001)$ MTJ (a) without the CoFe layer and (b) with the CoFe layer. The data for the as-prepared MTJs are denoted with the triangles (△), and the data for the MTJs annealed were denoted with open circles (○). (c) The annealing temperature T_a dependence of the TMR ratio for the MTJ with and without the CoFe layer measured at RT.

investigated epitaxial $Co_{1-x}Mn_x/MgO/Co_{1-x}Mn_x(001)$ MTJs with different x. Hereafter, we focus on the MTJ with $x = 0.25$ stacking which showed the best TMR effect: substrate/Cr(40)/Co_3Mn(10)/MgO(2.4)/Co_3Mn(4)/Co_3Fe(0, 1.5)/IrMn(10)/Ru(5) (thickness is in nm). The data for the MTJs with different x will be described in detail elsewhere. A thin CoFe alloy layer on the top Co_3Mn electrode was used to enhance the exchange bias of IrMn. All layers were deposited at RT, and in situ postdeposition annealing was performed for Cr and Co_3Mn at 700 and 200°C, respectively. Structure analysis was conducted using X-ray diffraction analysis (XRD) and transmission electron microscopy (TEM). Magnetization measurement was carried out using a vibrating sample magnetometer (VSM) and superconducting quantum interference device (SQUID) magnetometer. The microfabrication of the MTJs was performed using standard photolithography and Ar ion milling. Thirty-six junctions were obtained on the substrate with junction areas of 30×30, 20×20, or 10×10 μm^2. The MTJs were annealed for one hour in a vacuum furnace under an in-plane magnetic field of 5 kOe. Magnetoresistance (MR) measurements were carried out under in-plane magnetic field application with a four-probe method using a probe station at RT and a physical property measurement system (PPMS) at different temperatures.

Figures 1(a) and 1(b) show MR curves for the MTJ without and with the CoFe layer, respectively, and Fig. 1(c) shows those TMR ratios as a function of the MTJ annealing temperature T_a. Here, the TMR ratio is defined as the junction resistance change divided by the resistance for the parallel state of the magnetization R_p. The as-prepared MTJs have no exchange bias, and the antiparallel configuration of the magnaetization for the MTJ is not realized, so the TMR ratio is small, as shown in Figs. 1(a) and 1(b). For $T_a = 250 - 350$°C in Fig. 1(c), the TMR ratio for the MTJ with the CoFe layer increases, likely due to removal of some structural imperfections related to the bulk and/or interface of the MgO barrier. The TMR ratio for the MTJ with the CoFe layer exhibits the maximum value, 240%, at $T_a = 350$°C, and it then drops at $T_a = 375$°C [Fig. 1(c)]. This deterioration of the TMR ratio may be due to atomic diffusion from the top and/or bottom layers, as observed in other cases.[45,47] In addition, it might be related to an irreversible change of the bcc crystalline structure to another structure in Co-Mn. Note that a single bcc phase for the 10-nm-thick $Co_3Mn(001)$ films on Cr(001) was maintained up to 400°C and then changed into fcc phase at $\simeq$ 450°C, suggested by the XRD and VSM measurements (See Fig. S1 in supplementary material). Although the MTJ without the CoFe layer shows a similar annealing dependence of the TMR ratio, its TMR ratio is slightly smaller [Fig. 1(c)]. This is because the exchange bias at the $Co_3Mn(001)$/IrMn interface is not strong enough to stabilize the antiparallel state of the magnetizations, as seen in Fig. 1(a) and as also observed in other MTJs with different MgO barrier thicknesses (Fig. S2 in supplementary material).

The temperature dependence of the MR curves and the TMR ratio for the MTJ annealed at $T_a = 325$°C are shown in Figs. 2(a) and 2(b), respectively. Here, the sample is different from that shown in Fig. 1, although the stacking and fabrication conditions are identical. The TMR ratio is 634% at 5 K and rapidly decreases to 229% at 300 K with increasing temperature. The bias voltage V dependence of the TMR ratio for the same MTJ is also shown in Fig. 2(c). Here, a positive bias $+V$ means that the current $+I$ flows from the top electrode to the bottom. For both positive and negative bias V, the TMR ratios sharply and significantly drop within approximately ±0.1 V.

Figure 3 shows a representative cross-sectional TEM image of the MTJs after annealing. MgO(001) is epitaxially grown on the bottom $Co_3Mn(001)$ electrode, and the top $Co_3Mn(001)$ electrode is also epitaxially grown on the MgO(001) barrier. Thus, we confirm the presence of the lattice coherence at the interfaces in the MTJ, which is a prerequisite for the coherent tunneling mechanism. Note that the contrast between the top and bottom Co_3Mn layers mainly stem from the TEM sample preparation process and measurement condition and do

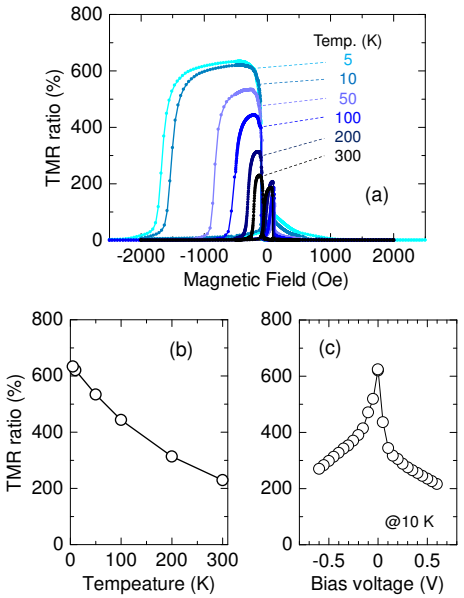

Fig. 2. (a) The MR curves measured at different temperatures, (b) the temperature dependence, and (c) the bias voltage dependence of the TMR ratio for the Co_3Mn/MgO/Co_3Mn(001) MTJ with the CoFe layer and $T_a = 325°C$.

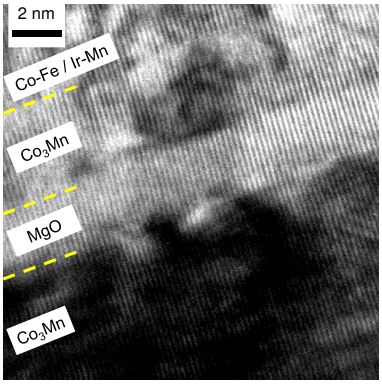

Fig. 3. A cross-sectional TEM image of the Co_3Mn/MgO/Co_3Mn(001) MTJ with the CoFe layer and $T_a = 325°C$.

not affect the structural information obtained from the TEM images.

Figure 4 shows the band dispersion along the <001> axis for bcc Co_3Mn calculated from first principles using spin-polarized relativistic Korringa-Kohn-Rostoker (SPR-KKR) code.[48] We adopted coherent potential approximation (CPA) to take the effect of substitutional atomic random alloy disorder into account. The exchange-correlation term was treated within the generalized gradient approximation.[49] The angular momentum cut-off l_{max} in the multiple scattering expansion was 3, and the 90 energy points on the complex energy path were used for the self-consistent calculation. For the Brillouin zone integration, we used 1330 irreducible k-points. The lattice constant a of 0.285 nm was used in this calculation.[33,36] In Fig. 4, although the energy levels are broadened due to the alloy disorder, the basic feature near the Fermi level E_F is similar to that of bcc Fe and

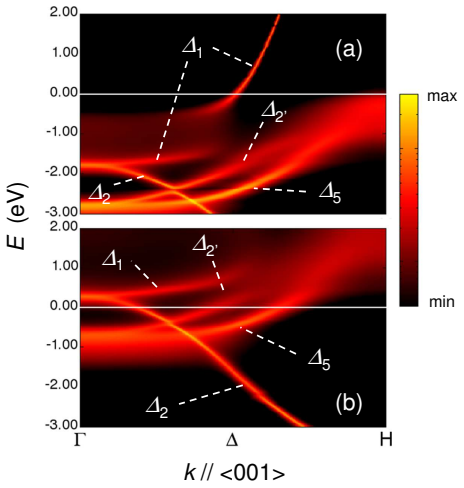

Fig. 4. The band structure of bcc Co_3Mn disordered alloys calculated from first principles for (a) a majority spin state and (b) a minority spin state. The energy $E = 0$ corresponds to the Fermi level E_F.

Co. There is a Δ_1 state at E_F for the majority spin and are no Δ_1 states at E_F for the minority spin. Thus, we expect coherent tunneling of the highly spin polarized Δ_1 bands in bcc Co_3Mn, as in bcc Fe, Co, and those alloys, as a primary requirement to obtain a high TMR ratio, in particular at LT.[23,24]

However, there are some differences near E_F in the band dispersions between bcc Co and bcc Co_3Mn. For the case of bcc Co, the Δ_1 band is only the state occupied at E_F for the majority spin, and E_F is located just below the bottom edge of the Δ_1 band at the Γ point for the minority spin; thus, a huge TMR effect was expected.[26] As seen in Fig. 4(a), in contrast, the E_F in bcc Co_3Mn touches the top edges of the heavily broadened $\Delta_{2'}$ and Δ_5 bands, which tends to reduce the TMR ratio compared with that of the bcc Co/MgO/Co(001) MTJs, as discussed for Fe/ MgO/Fe(001) MTJs.[23,26] Moreover, in Fig. 4(b), the bottom edge of the Δ_1 band for the minority spin is broadened by the alloy disorder, and finite electron states likely exist at E_F, which can reduce the spin polarization of the Δ_1 band as well as the TMR ratio, as originally discussed for MgO-based MTJs with bcc FeCo(001) disordered alloy electrodes.[13,14,50,51] Hence the above-mentioned differences in the electronic structures may reduce the TMR ratio from the predicted value of bcc Co/MgO/Co(001) MTJs. Note that it is yet unclear whether an interface resonance state (IRS) exists at the interface of bcc Co_3Mn(001) and MgO(001) even though the IRS could further degrade the TMR ratio, as discussed in the Fe/MgO/Fe(001) MTJs.[13,14,23,26]

The other source of the reduction of the TMR ratio would be a misfit dislocation generated at the top and bottom interfaces of the MgO barrier, as examined in the past.[52,53] For example, the lattice mismatch of about 3.4 % for Fe(001)/MgO(001) was reduced to about 3.1% for $Fe_{0.9}V_{0.1}$(001)/MgO(001) by doping V into the Fe electrode.[52,53] Consequently, the TMR ratio was enhanced with reducing the misfit dislocation density.[52,53] In our case, the lattice mismatch for bcc Co_3Mn(001) (a=0.285

nm) and MgO(001) is 4.5%. Although this mismatch is better than 5.3-5.6% in bcc Co(001) (a=0.282-0.283 nm)[28,29] and MgO(001) (a=0.4212 nm), it is not small enough to form the stacking without the misfit dislocations. Indeed, we found non-negligible number of the misfit dislocations in our MTJs, as qualitatively considered from the above-mentioned mismatch (See Fig. S3, supplementary material).

Finally we comment the relatively strong temperature and bias voltage dependence of the TMR effect, as observed, respectively, in Figs. 2(b) and 2(c) in this study. Those trends differ from the weak temperature and bias voltage dependence of the TMR ratio observed in MgO-based MTJs with the ultrathin bcc Co(001) electrodes.[27] A dominant origin in this study may be electron-magnon inelastic scattering at the interface.[54] This is because the theory for electron-magnon scattering predicts the large bias voltage dependence of the TMR ratio as well as the large temperature dependence of the TMR ratio, as experimentally observed in Figs. 2(c) and 2(b), respectively.[54] Electron-magnon scattering is determined by interface magnetism; thus, a detailed study of the interfaces will be a further subject. We note that the saturation magnetization for our bcc Co_3Mn film showed only about 7% reduction between 10 K and 350 K. The temperature dependence of the spin polarization is roughly scaled with that of the saturation magnetization,[55] thus the reduction of the spin polarization with elevating temperature would be a minor origin of the temperature dependence of the TMR ratio observed in this study.

In summary, MgO-based MTJs with the metastable bcc Co_3Mn(001) disordered alloy electrodes were studied. The TMR ratios of approximately 200–250% were obtained at RT and we successfully observed the TMR ratio greater than 600% at 10 K. This LT value was higher than the past experimental value[27] but much lower than the theoretical value in bcc Co/MgO/Co(001) MTJs.[26] Our theoretical calculation indicated that the spin polarization of the energy bands having the Δ_1 symmetries, which determine the coherent TMR effect, is relatively low in bcc Co_3Mn as compared with bcc Co. The TEM observations indicated that the number of misfit dislocations in our MTJs was not negligibly small. These would be responsible for the reduction of the TMR ratio compared to the TMR ratio predicted for bcc Co/MgO/Co(001) MTJs.

See supplementary material for the data of XRD and magnetization of the Co_3Mn films, the MgO barrier thickness dependence of the TMR ratio, and the cross-sectional TEM images showing the misfit dislocations.

T.T. and S.M. would like to thank T. Miyazaki and J. Okabayashi for valuable discussions. K.K., T.T. and S.M. would like to thank Y. Kondo and K. Saito for their technical assistances. This work was partially supported by JST CREST (No. JPMJCR17J5) and the JSPS Core-to-core program.

1) M. Julliere, Phys. Lett. A **54,** 225 (1975).
2) T. Miyazaki and N. Tezuka, J. Magn. Magn. Mater. **139,** L231 (1995).
3) J.S. Moodera, L.R. Kinder, T.M. Wong, and R. Meservey, Phys. Rev. Lett. **74,** 3273 (1995).
4) D.D. Djayaprawira, K. Tsunekawa, M. Nagai, H. Maehara, S. Yamagata, N. Watanabe, S. Yuasa, Y. Suzuki, and K. Ando, Appl. Phys. Lett. **86,** 092502 (2005).
5) S. Ikeda, J. Hayakawa, Y. Ashizawa, Y.M. Lee, K. Miura, H. Hasegawa, M. Tsunoda, F. Matsukura, and H. Ohno, Appl. Phys. Lett. **93,** 082508 (2008).
6) A. Sengupta and K. Roy, IEEE Trans. Circuits Syst. **63,** 2267 (2016).
7) Z. Chowdhury, J.D. Harms, S.K. Khatamifard, M. Zabihi, Y. Lv, A.P. Lyle, S.S. Sapatnekar, U.R. Karpuzcu, and J.-P. Wang, IEEE Comput. Archit. Lett. **17,** 42 (2018).
8) M. Zabihi, Z.I. Chowdhury, Z. Zhao, U.R. Karpuzcu, J.-P. Wang, and S.S. Sapatnekar, IEEE Trans. Comput. **68,** 1159 (2019).
9) J. Faure-Vincent, C. Tiusan, E. Jouguelet, F. Canet, M. Sajieddine, C. Bellouard, E. Popova, M. Hehn, F. Montaigne, and A. Schuhl, Appl. Phys. Lett. **82,** 4507 (2003).
10) S. Yuasa, T. Nagahama, A. Fukushima, Y. Suzuki, and K. Ando, Nat. Mater. **3,** 868 (2004).
11) S.S.P. Parkin, C. Kaiser, A. Panchula, P.M. Rice, B. Hughes, M. Samant, and S.-H. Yang, Nat. Mater. **3,** 862 (2004).
12) S. Yuasa, T. Katayama, T. Nagahama, A. Fukushima, H. Kubota, Y. Suzuki, and K. Ando, Appl. Phys. Lett. **87,** 222508 (2005).
13) F. Bonell, T. Hauet, S. Andrieu, F. Bertran, P. Le F 竪 vre, L. Calmels, A. Tejeda, F. Montaigne, B. Warot-Fonrose, B. Belhadji, A. Nicolaou, and A. Taleb-Ibrahimi, Phys. Rev. Lett. **108,** 176602 (2012).
14) S. Andrieu, L. Calmels, T. Hauet, F. Bonell, P. Le F 竪 vre, and F. Bertran, Phys. Rev. B **90,** 1 (2014).
15) C. Bellouard, Y. Lu, A. Duluard, B. Negulescu, C. Senet, N. Maloufi, M. Hehn, and C. Tiusan, Phys. Rev. B **98,** 144437 (2018).
16) K. Yakushiji, A. Sugihara, T. Nakano, and S. Yuasa, Appl. Phys. Lett. **115,** 202403 (2019).
17) Q. Xiang, H. Sukegawa, M. Belmoubarik, M. Al-Mahdawi, T. Scheike, S. Kasai, Y. Miura, and S. Mitani, Adv. Sci. **6,** 2 (2019).
18) Y. Sakuraba, M. Hattori, M. Oogane, Y. Ando, H. Kato, A. Sakuma, T. Miyazaki, and H. Kubota, Appl. Phys. Lett. **88,** 192508 (2006).
19) N. Tezuka, N. Ikeda, F. Mitsuhashi, and S. Sugimoto, Appl. Phys. Lett. **94,** 1 (2009).
20) W. Wang, H. Sukegawa, R. Shan, S. Mitani, and K. Inomata, Appl. Phys. Lett. **95,** 182502 (2009).
21) H. Liu, T. Kawami, K. Moges, T. Uemura, M. Yamamoto, F. Shi, and P.M. Voyles, J. Phys. D. Appl. Phys. **48,** 164001 (2015).
22) B. Hu, K. Moges, Y. Honda, H. Liu, T. Uemura, M. Yamamoto, J. Inoue, and M. Shirai, Phys. Rev. B **94,** 094428 (2016).
23) W.H. Butler, X.-G. Zhang, T.C. Schulthess, and J.M. MacLaren, Phys. Rev. B **63,** 054416 (2001).
24) J. Mathon and A. Umerski, Phys. Rev. B **63,** 220403 (2001).
25) I. Galanakis, P.H. Dederichs, and N. Papanikolaou, Phys. Rev. B **66,** 174429 (2002).
26) X.-G. Zhang and W.H. Butler, Phys. Rev. B **70,** 172407 (2004).
27) S. Yuasa, A. Fukushima, H. Kubota, Y. Suzuki, and K. Ando, Appl. Phys. Lett. **89,** 042505 (2006).
28) G.A. Prinz, Phys. Rev. Lett. **54,** 1051 (1985).
29) Y.U. Idzerda, W.T. Elam, B.T. Jonker, and G.A. Prinz, Phys. Rev. Lett. **62,** 2480 (1989).
30) F. Scheurer, B. Carri 竪 re, J.. Deville, and E. Beaurepaire, Surf. Sci. **245,** L175 (1991).
31) T. Nozaki, H. Kubota, A. Fukushima, and S. Yuasa, Appl.

Phys. Lett. **106,** 022405 (2015).
32) A.Y. Liu and D.J. Singh, Phys. Rev. B **47,** 8515 (1993).
33) D. Wu, G.L. Liu, C. Jing, Y.Z. Wu, D. Loison, G.S. Dong, X.F. Jin, and D.-S. Wang, Phys. Rev. B **63,** 214403 (2001).
34) L. Zhang, D. Basiaga, J.R. O'Brien, and D. Heiman, J. Appl. Phys. **98,** 106101 (2005).
35) R.J. Snow, H. Bhatkar, A.T. N'Diaye, E. Arenholz, and Y.U. Idzerda, J. Magn. Magn. Mater. **419,** 490 (2016).
36) K. Kunimatsu, T. Tsuchiya, K. Elphick, T. Ichinose, K.Z. Suzuki, A. Hirohata, and S. Mizukami, Jpn. J. Appl. Phys. **58,** 080908 (2019).
37) J.S. Kouvel, J. Phys. Chem. Solids **16,** 107 (1960).
38) M. Matsui, T. Ido, K. Sato, and K. Adachi, J. Phys. Soc. Japan **28,** 791 (1970).
39) A. Z. Menshikov, G. A. Takzei, Yu. A. Dorofeev, V. A. Kazan- stev, A. K. Kostyshin, and I. I. Sych, Zh. Eksp. Teor. Fiz. **89,** 1269 (1985) [Sov. Phys. JETP **62,** 734 (1985)].
40) K. Ishida and T. Nishizawa, Bull. Alloy Phase Diagrams **11,** 125 (1990).
41) Y. Goto, M. Araki, N. Takahashi, T. Yanase, T. Shimada, M. Tsujikawa, M. Shirai, A. Kamimaki, S. Iihama, S. Mizukami, and T. Nagahama, Jpn. J. Appl. Phys. **57,** 120302 (2018).
42) Y. Goto, T. Yanase, T. Shimada, M. Shirai, and T. Nagahama, AIP Advances **9,** 085322 (2019).
43) K.Z. Suzuki, R. Ranjbar, J. Okabayashi, Y. Miura, A. Sugihara, H. Tsuchiura, and S. Mizukami, Sci. Rep. **6,** 30249 (2016).
44) K.Z. Suzuki, Y. Miura, R. Ranjbar, L. Bainsla, A. Ono, Y. Sasaki, and S. Mizukami, Appl. Phys. Lett. **112,** 062402 (2018).
45) L. Bainsla, K.Z. Suzuki, M. Tsujikawa, H. Tsuchiura, M. Shirai, and S. Mizukami, Appl. Phys. Lett. **112,** 052403 (2018).
46) K.Z. Suzuki, S. Kimura, H. Kubota, and S. Mizukami, ACS Appl. Mater. Interfaces **10,** 43305 (2018).
47) T. Tsuchiya, T. Roy, K. Elphick, J. Okabayashi, L. Bainsla, T. Ichinose, K.Z. Suzuki, M. Tsujikawa, M. Shirai, A. Hirohata, and S. Mizukami, Phys. Rev. Mater. **3,** 084403 (2019).
48) H. Ebert, D. Kdderitzsch, and J. Minr, Rep. Prog. Phys. **74,** 96501 (2011).
49) J. P. Perdew, K. Burke, and M. Ernzerhof, Phys. Rev. Lett., **77**, 3865 (1996).
50) P.X. Xu, V.M. Karpan, K. Xia, M. Zwierzycki, I. Marushchenko, and P.J. Kelly, Phys. Rev. B **73,** 180402 (2006).
51) C. Franz, M. Czerner, and C. Heiliger, Phys. Rev. B **88,** 1 (2013).
52) F. Bonell, S. Andrieu, F. Bertran, P. Lefevre, A.T. Ibrahimi, E. Snoeck, C.-V. Tiusan, and F. Montaigne, IEEE Trans. Magn. **45,** 3467 (2009).
53) F. Bonell, S. Andrieu, C. Tiusan, F. Montaigne, E. Snoeck, B. Belhadji, L. Calmels, F. Bertran, P. Le F 竪 vre, and A. Taleb-Ibrahimi, Phys. Rev. B **82,** 092405 (2010).
54) S. Zhang, P.M. Levy, A.C. Marley, and S.S.P. Parkin, Phys. Rev. Lett. **79,** 3744 (1997).
55) C.H. Shang, J. Nowak, R. Jansen, and J.S. Moodera, Phys. Rev. B **58,** 2917(R) (1998).